INTERNATIONAL JOURNAL FOR NUMERICAL AND ANALYTICAL METHODS IN GEOMECHANICS
Int. J. Numer. Anal. Meth. Geomech. 2015
Published online in Wiley Online Library (wileyonlinelibrary.com). DOI: 10.1002/nag.2373

Thermal stresses in borehole heat exchangers

Selçuk Erol and Bertrand François*,†

Université Libre de Bruxelles (ULB) Building, Architecture and Town Planning Department (BATir), Laboratoire de GéoMécanique, Avenue F.D. Roosevelt, 50-CPI 194/2, B–1050, Bruxelles, Belgium

SUMMARY

The backfilling materials of borehole heat exchangers (BHE), particularly the grout material, must provide a suitable thermal contact and ensure durability to the induced thermal stresses because of the heat loading. In this paper, the thermal stresses that occurred in BHEs because of heat injection or extraction is investigated with an analytical solution of a hollow cylinder model that is adapted for time-dependent heat loading, the geometry of a BHE, and the thermo-mechanical properties of surrounding ground conditions. Firstly, the hollow cylinder model is solved with the considered boundary conditions in 2D plane stress. Secondly, the temperature differences at the inner and outer circles of the cylinder are evaluated with the heat line source models for continuous and discontinuous loading to observe the impact of the heat loading schedule. The developed analytical solution for thermal stress investigation is validated with numerical models. It is demonstrated that the analytical solutions agree well with numerical results for two types of BHE configurations (co-axial and single U-shaped pipes). Furthermore, the calculated maximum stresses are compared with the tensile strength of grout materials obtained from Brazilian tests. It is predicted that the thermal contraction of the grout, partially constrained by the surrounding rock, generates tensile stresses that may lead to cracking in the BHE. According to the results, the stiffness of rock has a primary role on the developed tensile stresses, and the relationship between the thermal conductivity of the ground and of the grout induces a proportional impact on the magnitude of thermal stresses. Copyright © 2015 John Wiley & Sons, Ltd.

Received 27 August 2014; Revised 9 January 2015; Accepted 5 February 2015

KEY WORDS: ground source heat pump; thermal stress; hollow cylinder; analytical solution; borehole heat exchanger

1. INTRODUCTION

Ground source heat pump (GSHP) systems are used for heating or cooling operations of buildings by exchanging heat between the buried borehole heat exchangers (BHEs) and the surrounding ground, and installed either in a heat advection-dominated aquifer system, which is driven by groundwater flow, or in heat conduction-dominated rock layers. Basically, a BHE comprises the geothermal high density polyethylene (HDPE) pipes in which anti-freeze mixture circulates through the borehole and surrounding empty space between pipes and the ground filled with grout mix to sustain superior heat transfer. During the heating or cooling operations, the comprised materials of BHE tend to dilate or contract. These deformations being partially constrained for vertically installed closed-loop BHE, thermal stresses are generated. In particular, when the system is operated under stiff rock layers, the BHE is extremely constrained, and temperature dropping (in case of heat extraction from the ground) leads to excessive tensile stress.

*Correspondence to: Bertrand François, Université Libre de Bruxelles (ULB) Building, Architecture and Town Planning Department (BATir), Laboratoire de GéoMécanique, Avenue F.D. Roosevelt, 50-CPI 194/2, B-1050 Bruxelles, Belgium.
†E-mail: bertrand.francois@ulb.ac.be

With regard to the thermal stress investigation of GSHP systems, several investigations have been reported about the impact of heating and cooling processes of axial stress and strain of energy piles ([1–5]). Laloui *et al*. [1] investigated *in situ*, the behavior of a heat exchanger pile subjected to the thermo-mechanical loading under the maximum thermal loading. As a consequence, the thermal loading has a greater impact on the axial stress of a pile more than the weight of construction. Di Donna *et al*. [4] studied numerically the effects of thermal cycles on the energy pile and surrounding soil for the stress and the displacements of piles in long-term operations. As a summary considered to the failure of the concrete, they concluded that the effects of thermal loading on the piles are admissible for the normal operation conditions. However, all of the approaches dealing with thermal stresses in heat exchanger piles focus on the integrity of the pile as a structural element. They consider the pile as a beam in which global normal forces evolve as a function of the applied forces, the soil-pile interaction, and the temperature of the pile. To our best knowledge, none of them investigated the effect of temperature distribution in the pile section on the generated thermal stresses.

In the case of single U-shaped pipe BHE, Allan and Philippacopoulos [6] preliminarily studied the deformation and stress fields in the complete pipe/grout/formation system through 2D numerical models. Furthermore, Philippacopoulos and Berndt [7] analyzed numerically the structural performance of the casing/grout/formation interaction of the deep geothermal wells with considerably higher temperature range compared with the GSHP systems installed in the shallow underground enthalpy. They summarized that the stress development mostly depends on the far-field stress, the stiffness of the grout, and the thermal loading. They concluded that the stiffer grout is not always appropriate for installation.

In order to investigate such a scenario of a BHE-installed underground, except an experimental approach, numerical models can handle to describe the detailed representations of complex BHE geometry and also to set extensively the thermo-mechanical properties of pipe, grout, and ground. In the framework of finite element methods (numerical models), these complex variations are carried out with several coupled studies by using the governing partial differential equations of the linear thermo-elasticity and heat transfer. Instead of using numerical methods, by simplifying the complex BHE geometry, it is feasible to approximate the thermal stress problem similarly with an analytical model. The analytical solution of hollow cylinder is used in different research fields to evaluate the mechanical and thermal stresses in materials [8–11].

Similarly, if the stresses in grouting material of a BHE induced by temperature gradient can be estimated by an analytical model, the thermo-mechanical problem will be described with a convenient approach, but, certainly, the assumed analytical model cannot provide precisely the stress components, as well as a numerical model in which a complete shape of BHE is defined. In some studies, such a similar simplification method for the geometry of BHE is used to analyze parameter estimation of soil [12] or to handle the changes on the rate of heat exchange through an interrupted thermal response test procedure [13].

The aim of this present study is:

- To represent an analytical model which evaluates thermal stresses arising on the grout material of a BHE, by taking into account the mechanical properties of the ground. Therefore, the stresses can be calculated as a function of the grout properties, the thermal loading, and the stiffness of rock. The generalized solution of thermal stresses in a hollow cylinder is already provided in the literature. The existing model is modified according to the boundary conditions of the assumed BHE and the ground. Because the contraction is assumed unconstrained on the z axis of BHE (i.e., the stresses in z direction being assumed constant), the study is carried out on 2D plane stress.
- Furthermore, the presented analytical model is used to investigate thermal stresses in the vicinity of a BHE under different geological conditions and its impact on two different commercial grouting materials (i.e., silica-sand based and calcite-based). The calculated stress components caused by the thermal loading are compared with the failure criterion obtained from tensile and compression strength results.

DOI: 10.1002/nag

2. ANALYTICAL MODEL OF THERMAL STRESS

The global problem is addressed as the combination of two hollow cylinder problems. The first one corresponds to the grout while the second one is to the rock. The assumed boundary conditions of the two combined problem are as follow (Figure 1):

- The internal boundary condition of the grout hollow cylinder for $r = r_a$ is free of stress. This condition assumes that the stiffness of the pipe is negligible in regards with the grout stiffness, which is a realistic assumption.
- At radius $r = r_b$, the radial stress and radial displacement of grout and rock are equal. This joined boundary condition (translating the mechanical equilibrium between the grout and the rock) makes that the two thermo-mechanical problems are coupled. Upon cooling of the ground (as considered here), the contraction of the grouting would generate likely a gap between rock and borehole, which has not been considered here. So, the adhesion between grouting and rock has been considered as strong as the resistance of the grouting itself. So, in practice, it could be expected that excessive tensile stresses would generate a detachment of the grout with respect to ground. This phenomenon would lead anyway to an unsafe situation because of the loss of axial waterproofness of the BHE and a decrease of the thermal transfers.
- At the semi-infinite far-field point of the rock, when $r \to \infty$, the stress and displacement are assumed unaffected by the temperature change in the near-field.
- Temperature change at the inner radius r_a is calculated as time-dependent, with a line source model which takes into account the thermal resistance of grout and the heat exchange rate. The temperature change at the outer radius r_b is determined with respect to the calculated heat source temperature and its proportional temperature gradient through the outer radius.

The mechanical conditions are considered in Section 2.1, Appendix A and Appendix B, while the temperature conditions are detailed in Section 2.2 and 2.3.

The initial condition is assumed upon zero stress, meaning that the initial overburden pressure has not been considered. Consequently, the result obtained in the succeeding section corresponds to a point located at low depth. Actually, upon cooling, the most critical situation is at low depth because the initial compressive stress is low and does not compensate the tensile stress induced by cooling. Also, the residual stress induced by the installation of the fresh grouting and its solidification has not been considered.

2.1. Axisymmetric thermal stresses in an hollow cylinder

Before presenting the specific applications with the two combined hollow cylinders, this section compiles the main thermo-mechanical equations applied to the hollow cylinder geometry upon plane stress conditions [14–16]. The momentum equilibrium equation in cylindrical coordinates for axisymmetric plane stress problem reads:

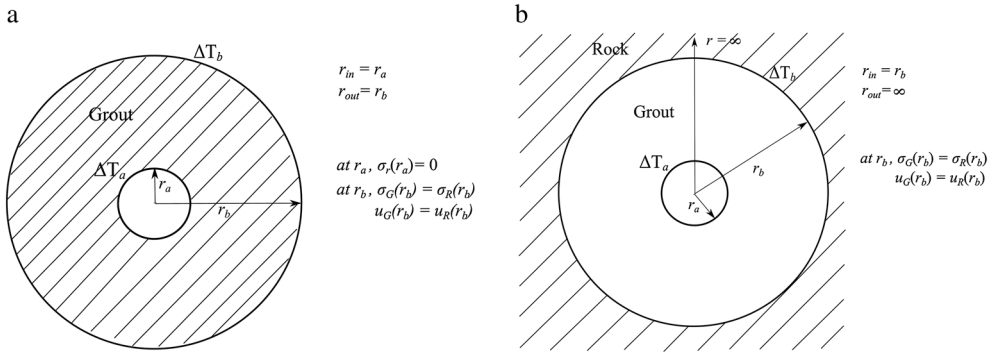

Figure 1. Illustration of two combined hollow cylinder problems: a) the grout and b) the rock.

DOI: 10.1002/nag

$$\frac{\partial \sigma_r}{\partial r} + \frac{1}{r}(\sigma_r - \sigma_\theta) = 0 \tag{1}$$

in which σ_r, σ_θ are the radial and tangential stresses, respectively. The r is the radial distance. The strain tensor components can be expressed as [14]:

$$\varepsilon_r = \frac{\partial u_r}{\partial r}, \quad \varepsilon_\theta = \frac{1}{r} u_r \tag{2}$$

where u_r is the radial displacement.

The stress–strain relationship upon non-isothermal conditions in cylindrical coordinates for linear thermo-elastic and isotropic material are given according to the generalized Hooke's law in 2D plane-stress equations as follows [15]:

$$\sigma_r = \frac{E}{1-v^2}(\varepsilon_r + v\varepsilon_\theta - \alpha\Delta\mathrm{T}(1+v)) \tag{3}$$

$$\sigma_\theta = \frac{E}{1-v^2}(\varepsilon_\theta + v\varepsilon_r - \alpha\Delta\mathrm{T}(1+v)) \tag{4}$$

where E is Young's modulus, υ is Poisson's ratio, and α is the coefficient of linear thermal expansion. The term, $\alpha\Delta\mathrm{T}(1+v)$, incorporates the thermal effect on the stress state. The sign convention assumes tensile stresses as positive.

By replacing the particular solution of the strain components into the stress equations (Eqs. 3 and 4) and setting them into the momentum equilibrium equation (Eq. 1), the derivation gives the displacement u_r as a function of radius with two integral constants, which will be solved with respect to the defined boundary conditions. The radial and tangential strains can be obtained with particular solutions given in Eq. 2, with respect to the derived displacement u_r; afterwards, the strain components can be set in Eqs. 3 and 4. The full derivation is provided in Appendix A.

The stresses are obtained as:

$$\sigma_r = E\left(\frac{A}{1-v} - \frac{\alpha S}{r^2} - \frac{B}{(1+v)r^2}\right) \tag{5}$$

$$\sigma_\theta = E\left(\frac{A}{1-v} + \frac{\alpha S}{r^2} + \frac{B}{(1+v)r^2} - \alpha\Delta\mathrm{T}\right) \tag{6}$$

in which A and B are the integral constants and S is the integration of the temperature difference ΔT, with respect to the radial distance r as shown in Eq. A3.

This set of equations is the general solution for a thermo-elastic problem of a hollow cylinder assuming axisymmetric distribution of temperature. The current problem is a combination of two combined hollow cylinder problems, as described in Figure 1. Consequently, four integration constants have to be determined: A_G and B_G for the grout problem and A_R and B_R for the rock problem. Subscripts G and R refer to the grout and the rock properties, respectively. For the sake of completeness, the determination of those constants according to the specific boundary conditions of the present problem is detailed in Appendix B.

Once the constants have been determined, the stress components of grout material depending on the mechanical properties of surrounding rock can be calculated as follows:

$$\sigma_{r,G} = \frac{E_G}{r^2}\left[\frac{A_G(r^2 - r_a^2)}{(1-v_G)} - \alpha_G S_G\right] \tag{7}$$

$$\sigma_{\theta,G} = \frac{E_G}{r^2}\left[\frac{A_G(r^2 + r_a^2)}{(1-v_G)} + \alpha_G S_G - \alpha_G\Delta\mathrm{T}r^2\right] \tag{8}$$

where A_G is given in Eq. B7.

DOI: 10.1002/nag

In a hollow cylinder submitted to an axisymmetric temperature field, the temperature distribution along the radius can be expressed as a function of the temperature at the two boundaries, as follows [15]:

$$\Delta \mathrm{T}(r,t) = \Delta \mathrm{T}_a(t)\frac{\ln\left(\frac{r_b}{r}\right)}{\ln\left(\frac{r_b}{r_a}\right)} + \Delta \mathrm{T}_b(t)\frac{\ln\left(\frac{r_a}{r}\right)}{\ln\left(\frac{r_a}{r_b}\right)} \tag{9}$$

where $\Delta \mathrm{T_a}$ and $\Delta \mathrm{T_b}$ are the temperature variations at the boundaries r_a and r_b, respectively, and they can be obtained as time-dependent for continuous and discontinuous heat loading as described in Sections 2.2 and 2.3. Typically, Eq. 9 assumes a steady-state condition. However, in our case, the time-dependent effect is taken into account through the temperature evolution at the boundaries of the problem ($\Delta \mathrm{T_a}(t)$ and $\Delta \mathrm{T_b}(t)$), the evolution of the temperature profile being treated as a succession of steady-state conditions. In fact, the achievement of this approach is valid because of the short distance from the heat source to the considered borehole wall, where the heat transfer reaches to equilibrium within a short time. The rate of temperature change in the pipe remains low, with respect to the speed of thermal transfer in the grout which makes that the thermal profile can be seen as a succession of steady-state profile.

2.2. *Continuous constant heat load*

For the thermal stress calculations in a hollow cylinder, initially, the temperature change is time-dependent and at $t = 0$, the domain is in a state of uniform temperature and stress. The GSHP systems are operated by fixing the heat extraction rate, and neither the fluid temperature nor the borehole wall temperature is constant. In order to obtain the temperature changes at the inner circle r_a as a time-dependent solution, a line source analytical model described for the heat transfer between borehole and the infinite region can be used. The inner circle temperature (i.e., heat source) as a function of time is given as [17]:

$$\Delta \mathrm{T}_a(t) = \frac{q_L}{4\pi\lambda_R}\mathrm{E}_1\left(\frac{r_b^2}{4D_R t}\right) + q_L R_{G-C} \tag{10}$$

in which q_L is the heat exchange rate (assuming the sign is negative for heat extraction from the ground), λ_R is the thermal conductivity of rock, r_b is the radius of borehole, D_R is the thermal diffusivity of rock, and $R_{G\text{-}C}$ is the thermal resistance of grout material which can be calculated as the thermal resistance of a hollow cylinder [18]:

$$R_{G-C} = \frac{\ln(r_b/r_a)}{2\pi\lambda_G} \tag{11}$$

where λ_G is the thermal conductivity of grout. Because the temperature difference between the heat source and the borehole wall is proportional to the heat exchange rate and the thermal resistance of grout, the temperature difference at the wall (outer circle, r_b) is calculated as follows [19]:

$$\Delta \mathrm{T}_b(t) = \Delta \mathrm{T}_a(t) - q_L R_{G-C} \tag{12}$$

The calculated temperature differences at the inner and outer radii (Eqs. 10 and 12) can be set in Eq. 9.

2.3. *Discontinuous heat extraction*

Alternatively, the thermal stress components can be also calculated under a discontinuous heat extraction condition, as the GSHP systems are operated depending on a heat extraction schedule depending on the annual operation hours provided by guidelines [20]. According to the schedule, the operation hours can vary daily and monthly, as well as the heat extraction rate. Recently, Erol *et al.*

DOI: 10.1002/nag

[21] developed a solution for discontinuous heat extraction by analytically convoluting rectangular function or pulses in time domain both for single and multi-BHEs field by using the Green's function, which is the solution of heat conduction/advection/dispersion equation in porous media. This solution can be also adapted at the scale of a BHE. By adding the term $q_L R_G$ to the equation, the temperature of the heat source can be evaluated for discontinuous heat extraction, as ΔT_a, and ΔT_b can be calculated without the term $q_L R_G$. In the analytical evaluation of the convolution equation, both the heat extraction rate q_L and f function are discretized with a differential of Δt. The convolution as a sum of impulse responses at coordinates (x, y, z) is given as:

$$\Delta T_a(x, y, z, t) = \sum_{i=0}^{n-1} q_L(i\Delta t) f(x, y, z, t - i\Delta t)\Delta t + q_L(i\Delta t) R_G \tag{13}$$

where n denotes the time span, $i\,\Delta t$ is the time delay of each unit impulse, and the delayed and shifted impulse response is $q_L\,(i\,\Delta t)\,f(t-i\,\Delta t)\,\Delta t$. The $f\,(x, y, z, t)$ function is convoluted with a rectangular heat extraction function $q_L(t)$, defined as follows:

$$q_L(t) = \begin{cases} q_L \text{ for } t \in [0, \mathbf{T}] \\ 0 \text{ otherwise} \end{cases} \tag{14}$$

where $\mathbf{T}$ is the period of heat extraction. According to Erol *et al.* [21], f function is the modified Green's function for heat conduction/advection/dispersion equation. However, because the study is considered under stiff rock ground condition for thermal stress analyses, the equation can be simplified by neglecting the advection/dispersion terms from the equation and can be written as:

$$f(x, y, z, t) = \frac{1}{8\pi t \lambda_R} \exp\left[-\frac{x^2}{\frac{4\lambda_R t}{\rho_R c_R}} - \frac{y^2}{\frac{4\lambda_R t}{\rho_R c_R}} \right] \left[erf\left(\frac{z}{\sqrt{\frac{4\lambda_R t}{\rho_R c_R}}} \right) - erf\left(\frac{z - H}{\sqrt{\frac{4\lambda_R t}{\rho_R c_R}}} \right) \right] \tag{15}$$

in which λ_R is the bulk thermal conductivity of rock and $\rho_R c_R$ is the bulk volumetric heat capacity of rock.

Once the temperature differences are calculated for discontinuous heat extraction at the inner circle of the cylinder with Eq. 13 as ΔT_a and ΔT_b obtained without the term $q_L R_G$, the values can be assigned in Eq. 9.

It is important to mention that the reference coordinate of Eqs. 10 and 13 is located on the heat source boundary conditions (i.e., at $r = r_a$). Consequently, the matching of the temperature field equations and the stress and displacement field equations requires a shift of the radial coordinates of r_a.

3. NUMERICAL MODEL

The hollow cylinder analytical model for stress analyses is validated with the finite element software COMSOL Multiphysics (COMSOL, Burlington, MA, U.S.A). The study is represented by a 2D plane-stress homogeneous model domain of 3 m × 3 m (Figure 2a). Those dimensions are high enough to guarantee that the external boundaries do not impact the thermo-mechanical results in the vicinity of the hollow cylinder. The mesh is generated using uniform triangle elements. The hollow cylinder is located at the central position of the model domain and has an outer diameter of 0.14 m and the inner circle diameter is 0.026 m.

The edges of the model are constrained (displacement zero in all directions). The inner circle of hollow cylinder is free of normal stress. Heat flux is applied in the inner circle, while the external edge of the model is considered as adiabatic.

The problem is solved as time-dependent. Linear thermo-elastic behavior under plane stress conditions is considered with the thermal stress module, which couples the general heat transfer equation for solving the temperature change on the domain caused by thermal load and the static

DOI: 10.1002/nag

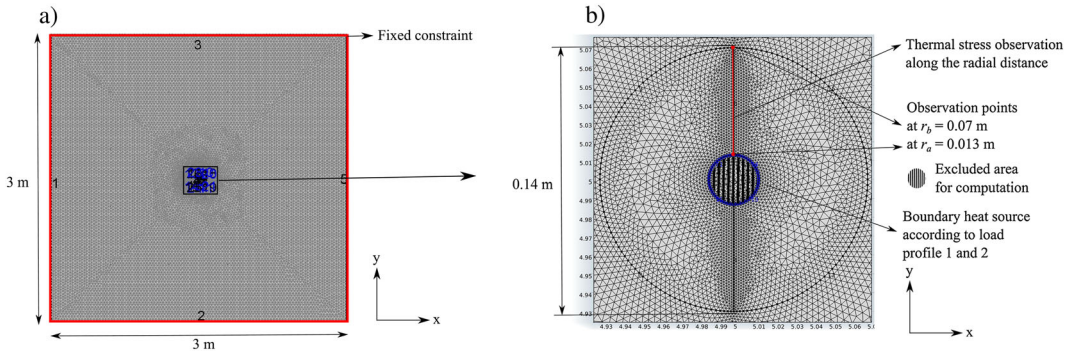

Figure 2. Sketch illustrating 2D plane stress numerical model: a) the model domain and b) the hollow cylinder model, according to the analytical assumption.

solid mechanics equations for the calculation of stress–strain relation due to the thermal expansion/contraction. The compressive stress due to depth (the overburden pressure) is not considered. The results are analyzed in terms of stress variations, and not in total stresses.

The initial temperature is 20 °C, and the simulation time is set to 120 h. In order to observe the difference of continuous and discontinuous heat loading rates on the stress field in grout material, the total amount of heat 2700 W m^{-1} h is injected in two different ways: (i) continuously through the simulation time as -22.5 W m^{-1} (Figure 3a) and (ii) as a discontinuous load profile distributed randomly in 120 h (Figure 3b). The heat extraction is considered as the heating of a house (i.e., cooling the ground).

4. MATERIAL PARAMETERS

In the present study, two types of grout material widely used for BHEs are considered in the experiments and took place in the calculations with their characteristics. One of the ready-made grout mixtures is thermally enhanced silica-sand-based material and the other one is calcite-based material with a lower thermal conductivity. The mechanical and thermal properties of grouting materials and geothermal HDPE pipes are given in Table I. The chemical compounds of different constituents of a grout material affect not only the strength of materials but also the thermal properties. The grout thermal conductivity influences the heat transfer, which in turn modifies the thermal gradient between the heat carrier fluid pipes and the ground and affects thermal stresses on the grouting material.

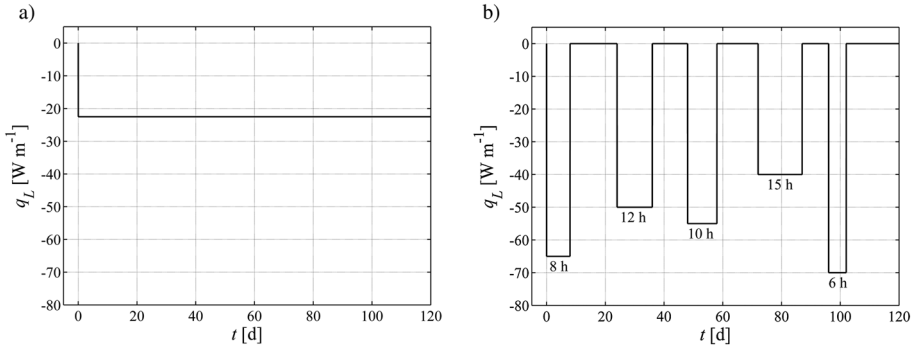

Figure 3. Load profiles of heat extraction of equal amount of heat 2700 W m^{-1} h as: a) continuous loading (load profile 1) and b) discontinuous loading (load profile 2).

DOI: 10.1002/nag

Table I. Parameters of laboratory setup components.

Parameters	Silica-sand based grout material	Calcite-based grout material	High density polyethylene pipe
α [K^{-1}] $\times 10^{-5}$	1.4[a]	1.3[a]	12[b]
E [Pa] $\times 10^{9}$	6.5[b]	5.5[b]	1.45[b]
υ [−]	0.21[b]	0.21[b]	0.45[b]
ρc [J kg^{-1} m^{-3}] $\times 10^{6}$	2.7[b]	2.5[b]	2[b]
λ [W m^{-1} K^{-1}]	2.3[b]	0.9[b]	0.42[b]

[a][22] depending on the dominant mineral in the admixture, [b][23], [c][24], [d][6], [e][25].

The validation of analytical solution is accomplished with two different varieties of rock stiffness by setting the Young's modulus of rock as 10 and 90 GPa. The thermo-physical parameters of rock in all varieties are set similarly. The characteristics of the rock are given in Table II.

5. VALIDATION

The analytical solution of hollow cylinder model is compared with the numerical model results for the two Young's modulus of rock under continuous and discontinuous load profiles. Consequently, four scenarios are investigated. Only silica-sand-based grout material is considered.

Temperature profiles seen in Figure 4 demonstrate that the line heat source solutions for both continuous (Eq. 10) and discontinuous heat loading (Eq. 13) provide a good agreement with numerical results. Despite that, the comparison results of discontinuous loading show a small discrepancy because of the time step discretization, which is taken likely larger for such a short time operation. The thermal resistance of cylinder calculated according to Eq. 11 is $R_{G\text{-}C} = 0.11\,\mathrm{K\,m\,W^{-1}}$. The comparison between continuous and discontinuous heat loading shows that the magnitude of the temperature gradient in the BHE strongly depends on the distribution of heat exchange rate over time. Even though the total amount of heat injected in 120 h is similar in both load profiles, the significant difference of peak temperature between the results is strongly impacted by the heat loading schedule. For continuous heat loading at 120th operation hour, the maximum temperature difference between inner and outer radius is 2.6 K (Figure 5a), while for discontinuous heat loading at the end of the fifth extraction cycle (i.e., 102nd h), we get 8.1 K (Figure 5b). This difference shows that the analytical solution for continuous heat extraction (Eq. 10), which is traditionally used in most of the studies for the analyses of thermal response test, cannot provide appropriate temperature profiles to investigate the impact of daily heat loading on considered grout material. Therefore, the validation of hollow cylinder solution is carried out for both load profiles, but the load profile 1 (i.e., continuous loading) is not used for further thermal stress investigation of BHE in the following sections.

For the hollow cylinder analytical model, the calculated temperature values shown in Figure 4 are set in Eq. 9 to obtain the stress components of grout material (Eqs. 7 and 8) under continuous and discontinuous heat loading. The analytically calculated thermal stresses seen in Figure 5 for the Young's modulus of 90 GPa of rock agree well with numerical model results. In the absence of the stress at the semi-infinite far field point of the rock, both stress components are subjected to tension.

Table II. Parameters of surrounding rock.

Parameters	Rock
α [K^{-1}]	0.8×10^{-5}[a]
E [GPa]	10/90[b]
υ [−]	0.25[b]
ρc [MJ kg^{-1} m^{-3}]	3[b]
λ [W m^{-1} K^{-1}]	3.2[b]

[a][26], [b][27], [c][28].

DOI: 10.1002/nag

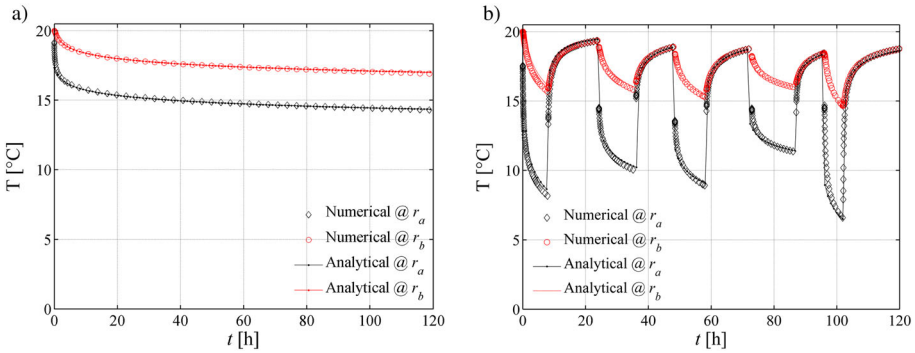

Figure 4. Comparison of temperature profiles as the result of: a) Load profile 1, according to Eq. 10 and b) Load profile 2, according to Eq. 13. The temperatures at r_b are calculated in the considered equations without the grout resistance term.

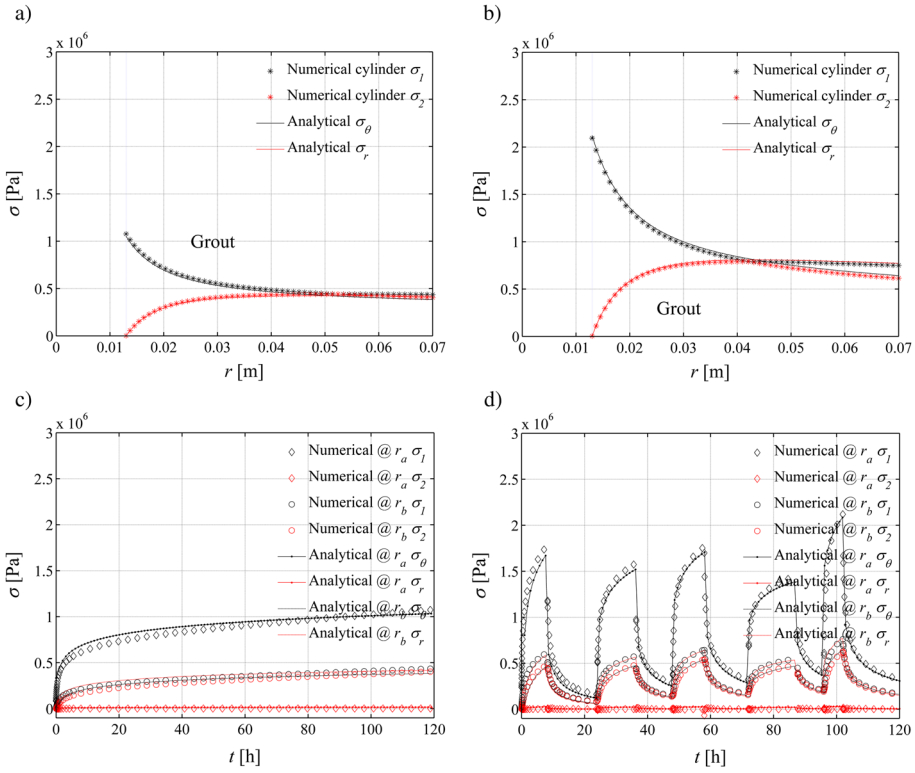

Figure 5. Validation of analytical solution with numerical results under the rock Young's modulus of 90 GPa: a) and b) stress over distance at the operation of: a) 120th hour b) 102nd hour (at the end of the 5th cycle). c) and d) stress over time. Shown in a) and c) are the results obtained for load profile 1; Shown in b) and d) are the results obtained for load profile 2.

Overburden pressure being not considered (i.e., the initial stress state is null), this tensile stress must be considered as a stress variation. The presence of overburden pressure would reduce the total tensile stress.

For low values of r, the tangential stress corresponds to the first principal stress, and the second principal stress is the radial stress. Further, for larger r, the principal stresses cross over each other and so, radial stress becomes the first principal stress.

In Figure 6, the stress components are calculated for lower elastic stiffness of rock compared with the stresses shown in Figure 5, but the similar temperature profiles are set. The analytical solution of

DOI: 10.1002/nag

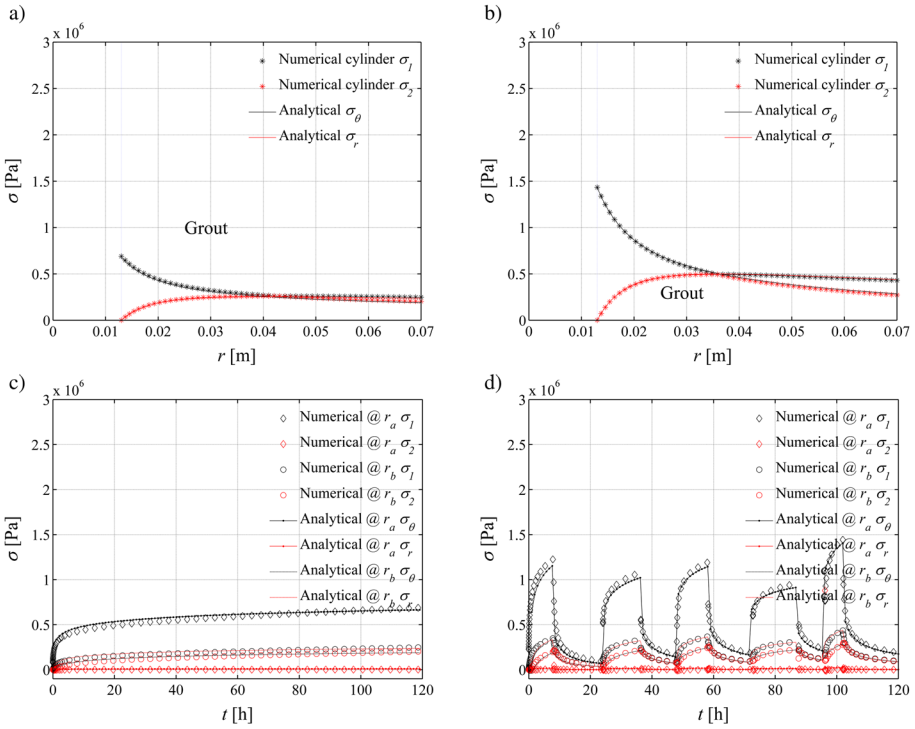

Figure 6. Validation of analytical solution with numerical results under the rock Young's modulus of 10 GPa: a) and b). Stress over distance at the operation of: a) 120th hour b) 102nd hour (at the end of the 5th cycle). Stress over time c) and d). Shown in. a) and c) are the results obtained for load profile 1. Shown in b) and d) are the results obtained for load profile 2.

hollow cylinder is in agreement with numerical model results and it verifies that the analytical model can evaluate the stress components depending on the Young's modulus of surrounding rock. Comparing results in Figures 5 and 6, when the rock is stiffer, the generated thermal stress is larger. This is because of the stronger restriction of the strain induced by stiffer rock.

For both cases (Figures 5 and 6), the magnitude of thermal stresses depends on the temperature gradient induced by the thermal loading. For discontinuous heat loading, the higher temperature gradient induces higher stresses. In Figures 5c and d and 6c and d, a small discrepancy can be seen on the prediction of tangential stress at r_a over time, but by the progression of time, the results match comparatively well. This can be accounted for Eq. 9, in which the Laplacian temperature change is calculated according to a succession of steady-state conditions. At short term, the rate of temperature change does not permit to catch perfectly the transient problem with a series of thermal equilibrium profile. However, the analytical approximation provides an acceptable matching.

6. HOLLOW CYLINDER APPROACH FOR A SINGLE U-SHAPED PIPE AND COAXIAL PIPE BOREHOLE HEAT EXCHANGER

6.1. Assumptions

In this section, the thermo-mechanical relationships developed for simplified hollow cylinder shape are extended to more realistic geometries of BHE. In particular, single U-shaped and co-axial pipes BHEs are considered. The simplified geometry differs from real BHE, mainly from two elements: the HDPE pipes are not represented in the simplified model and the geometry of single U-shaped BHE does not follow a hollow cylinder shape. If the pipe was considered, when the heat transfer reaches equilibrium between the internal heat load and the ground after a couple of hours, the temperature difference due to the pipe would not be significant, and the thermally-induced stresses that occurred in the pipes have a

DOI: 10.1002/nag

minor impact on the grout because the tension that occurred because of stiffer grout/rock dominates the motion. Therefore, the pipe is disregarded in this study and the temperature changes due to geometry difference is adapted to the analytical model, depending on the thermal resistance of single U-shaped pipe BHE and co-axial pipe BHE (Eqs. 16 and 21). For the geometry, U-shaped and co-axial pipes BHE will be considered, according to different assumptions:

For co-axial pipe BHE, it is obvious that the geometry is very similar to the hollow cylinder configuration. The hollow cylinder model is assumed from the interior wall of the outlet pipe to the borehole wall. The radial direction is simply taken along the radius of borehole (Figure 7b).

For the single U-shaped pipe, even if the geometry differs, it will be demonstrated that hollow cylinder approximation may still give satisfactory results. In the analytical model, the half of the BHE is disregarded; the heat flux in the pipe in which the fluid temperature is higher is assumed as the interior boundary of the hollow cylinder; and the borehole wall at where the temperature is symmetric can shape the exterior boundary of the cylinder. The radial direction is assumed to be the straight line joining the center of the pipe to the symmetric point on the borehole wall (Figure 7a). Likely, this cannot be the worst location to observe the stresses. However, this point is the only point where the temperature can be predicted with the heat line source model at the borehole wall.

In this section, the temperature profile used for the hollow cylinder model is modified according to the grout thermal resistance of different BHE configurations and compared with the numerical results. For the numerical model of both BHE configurations, the pipes are considered. The interior pipes are fixed as the heat source boundary according to the load profile 2 (i.e., discontinuous loading). The interior part of the pipes in which the heat carrier fluid circulates is excluded out of computation. The thermo-mechanical parameters of HDPE pipe and the silica-sand-based grout material set in BHE numerical model can be found in Table I. The parameters of rock are set as described in the previous chapter (Table II).

The most important part of this assumption is the method to determine the temperature change that can provide approximately the thermal stresses that occurred in the grout. The hollow cylinder analytical model does not take into account the stresses that occurred in the pipe of these BHE configurations. Therefore, the appropriated method is to calculate the temperature change only with the grout resistance.

The estimation of the grout resistance of a single U-shaped pipe BHE can be analytically obtained, regarding the geometry and the thermal characteristics of the BHE. The effective borehole resistance, excluding the convection and conduction pipe resistances, is given by Bennet *et al*. [29]. The provided solution for the single U-shaped pipe BHE is given as follows:

$$R_{G-U} = \frac{1}{4\pi\lambda_g}\left[\ln\left(\frac{a_1 a_2^{1+4\eta}}{2\left(a_2^4-1\right)^{\eta}}\right) - \frac{a_3^2\left(1-\frac{4\eta}{\left(a_2^4-1\right)}\right)^2}{1+a_3^2\left(1+\frac{16\eta}{\left(\left(a_2^4-1\right)/a_2^2\right)^2}\right)}\right] \tag{16}$$

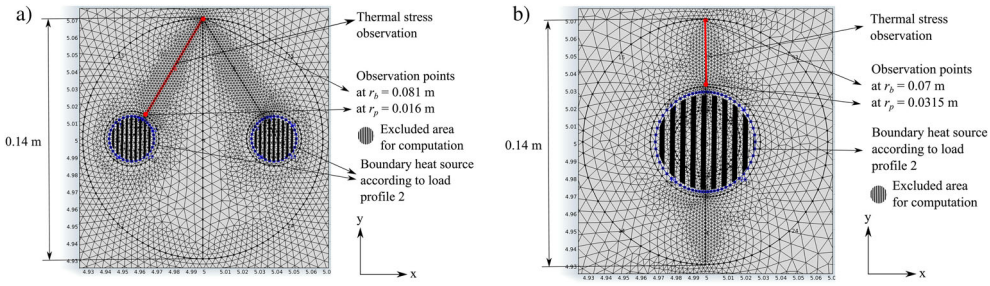

Figure 7. Numerical thermal stress analyses for comparison of the hollow cylinder analytical model with a) single U-shaped pipe borehole heat exchanger (BHE) model and b) coaxial pipe BHE model.

DOI: 10.1002/nag

in which a_1, a_2, a_3, and η are the dimensionless parameters as:

$$\eta = \frac{\lambda_g - \lambda_R}{\lambda_g + \lambda_R} \tag{17}$$

$$a_1 = \frac{r_b}{r_p} \tag{18}$$

$$a_2 = \frac{r_b}{x_c} \tag{19}$$

$$a_3 = \frac{r_p}{2x_c} \tag{20}$$

where r_b is the radius of borehole, r_p is the outer radius of pipe, and x_c is the half-shank spacing (the distance from the center of the pipe to center of BHE).

The grout thermal resistance of coaxial pipe BHE can be calculated similar to the thermal resistance of a hollow cylinder as:

$$R_{G-C} = \frac{\ln\left(r_b/r_p\right)}{2\pi\lambda_G} \tag{21}$$

For the analytical model, again, the stress components are calculated according to Eqs. 7 and 8. The temperature changes, ΔT_a, are calculated based on the grout resistance of considered configurations according to Eq. 13, and ΔT_b is evaluated typically in the same equation but without the term $q_L R_G$.

6.2. *Results*

For both of the BHE configurations, the temperature difference at r_a is calculated from Eq. 13, with the thermal resistance of silica-sand based grout theoretically estimated according to Eq. 16 for the single U-shaped pipe BHE ($R_{G\text{-}U} = 0.05\,\mathrm{K\,m\,W^{-1}}$) and Eq. 21 for the co-axial pipe BHE ($R_{G\text{-}C} = 0.055\,\mathrm{K\,m\,W^{-1}}$). The stresses in the pipe shown in Figures 8 and 9 are obtained only from numerical models. Therefore, the comparison is considered only in the grout.

The comparison results demonstrate that the analytical model of hollow cylinder is able to estimate nearly the thermal stresses on the grout material of the typical BHE configurations. The result obtained from the numerical model showing the stresses that occurred on the pipe is considerably larger than grout. This is likely because of the thermo-mechanical and thermo-physical characteristics of the pipe, because the thermal expansion of the pipe is ~10 times larger and the stiffness is 5 times smaller than the grouting material. The borehole resistance depending on the geometry and the thermal conductivity of grout reduces the thermally-induced stresses through a decrease of the temperature gradient in the grout.

The stress profiles shown in Figure 9, under the Young's modulus of 10 GPa of rock, show the small discrepancy of validation compared with the previous stresses in Figure 8. In fact, when the rock has low stiffness, the influence of pipe on the configuration of BHE becomes proportionally substantial. Although, in the grout material, the tangential stress is in agreement with the first principal stress, whereas the radial stress slightly mismatches with the secondary principal stress. However, because the radial stress on the grout has a minor impact close to the pipe, this conflicting result can be disregarded. Comparing the stresses obtained under the rock Young's modulus of 90 GPa shown in Figure 8 with the results in Figure 9, certainly, the stiffer rock has a larger impact on the grouting material. On the other hand, the thermal stress results of the pipes obtained only from the numerical model are nearly identical, although the stiffness of rock is significantly different. This effect is likely due to the identical thermal gradient between the applied heat load and the borehole wall

DOI: 10.1002/nag

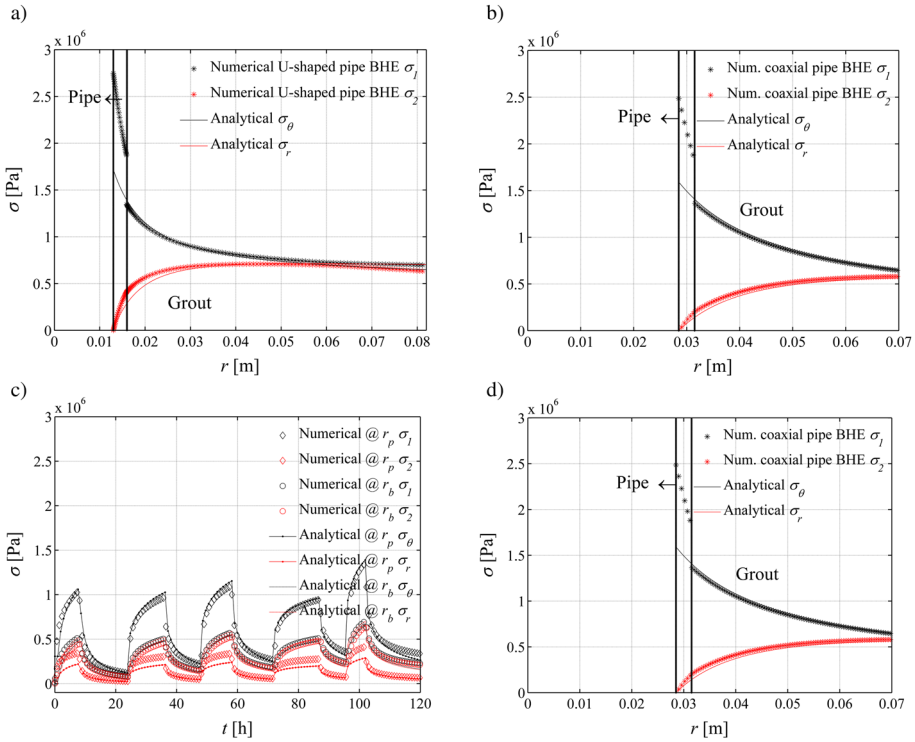

Figure 8. Comparison stress results of grout material under the rock Young's modulus of 90 GPa. Stress over distance at the operation of 102nd hour (at the end of the 5th cycle) a) and b). Stress over time. c) and d). Shown in a) and c) are the results for single U-shaped pipe borehole heat exchangers (BHE), Shown in b) and d) are the results of coaxial pipe BHE.

temperature. If the impact of the BHE configurations is analyzed, except the stresses that occurred on the pipe, the coaxial pipe BHE has a slightly steeper stress profile on the grout material along the radial distance compared with the single U-shaped pipe BHE, but the magnitude of the stress components that evolves is nearly similar over time at r_a and at r_b for both of the BHE configuration.

The results demonstrate that the adapted analytical model of hollow cylinder depending on the thermal resistance of different BHE configurations provides a good approximation of the thermal stress on the grout material. The results have been obtained according to a given cooling scenario (Figure 3b), which is representative of a real situation but which is definitely not the worst situation. A more rapid and more intensive cooling may produce higher tensile stresses that would be still more critical for the integrity of the BHE. In the following chapter, this analytical model is used further to evaluate the crack development on the grout under various scenarios, as a function of the tensile and compression strength of the grout.

7. THERMAL STRESS INVESTIGATION FOR BOREHOLE HEAT EXCHANGERS

7.1. Different scenarios

In order to approximate the failure of grouting material under thermal loading, the failure envelope can be plotted on the normal stress–shear stress plane using the uni-axial compression strength and tensile strength values obtained from experiments with the components of σ_1 and σ_2. The failure criterion surrounds the Mohr circles obtained from tensile and compression tests at failure. We assume that it is composed of two straight lines in the normal stress–shear stress plane. The shear failure is obtained according to the Mohr-Coulomb failure envelope that is tangent to the Mohr circles at failure from compression and tensile tests, while the tensile failure is represented by a 'cut-off' criterion corresponding to the tensile strength and unaffected by the shear stress (i.e., a vertical line

DOI: 10.1002/nag

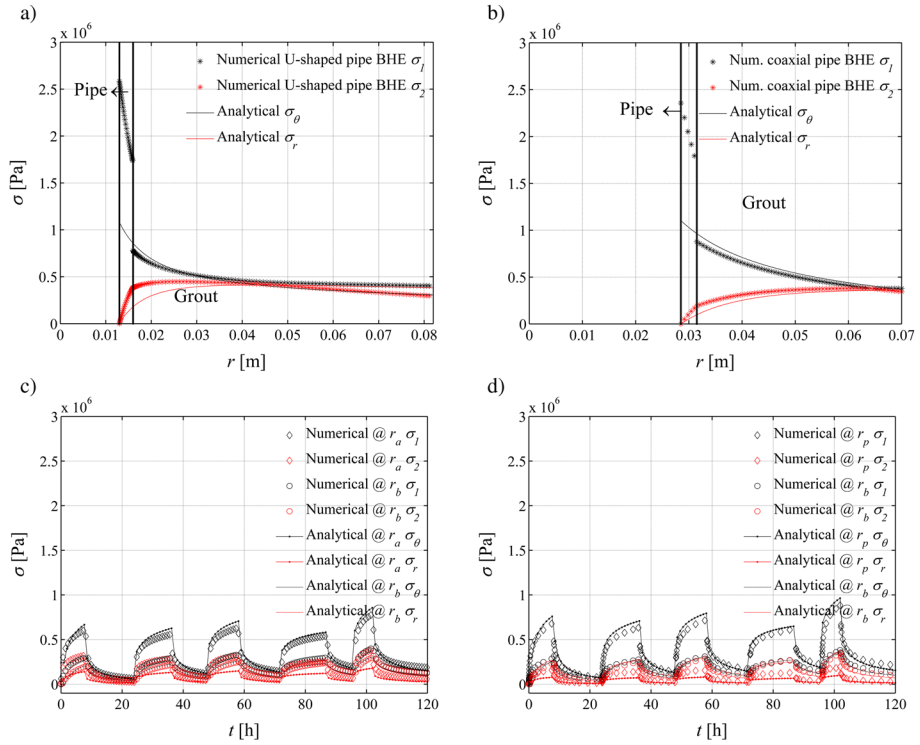

Figure 9. Comparison stress results of grout material under the rock Young's modulus of 10 GPa. Stress over distance at the operation of 102nd hour (at the end of the 5th cycle) a) and b). Stress over time c) and d). Shown in a) and c) are the results for single U-shaped pipe borehole heat exchanger (BHE). Shown in b) and d) are the results of coaxial pipe BHE.

in the normal stress–shear stress plane) (Figure 10). This tensile strength criterion has the merits of simplicity and ease-of-use when tensile strength from Brazilian test is known (see for instance [30], for application in rock mechanics).

Then, this failure criterion will be compared with the tangential and radial stresses due to thermal loading, which are obtained from analytical models. The discontinuous heat load profile is applied throughout 30 days with 8 h of daily extraction set to 60 W m^{-1} and, for the rest of the day, 16 h is left idle to observe how the stresses are evolving through the recovery phases of a BHE operation. The total amount of heat extracted for heating operation is ~9000 kW h for a BHE with a length of 100 m. This corresponds to 17 % of operation hours out of 1800 h allowed in a year for a BHE,

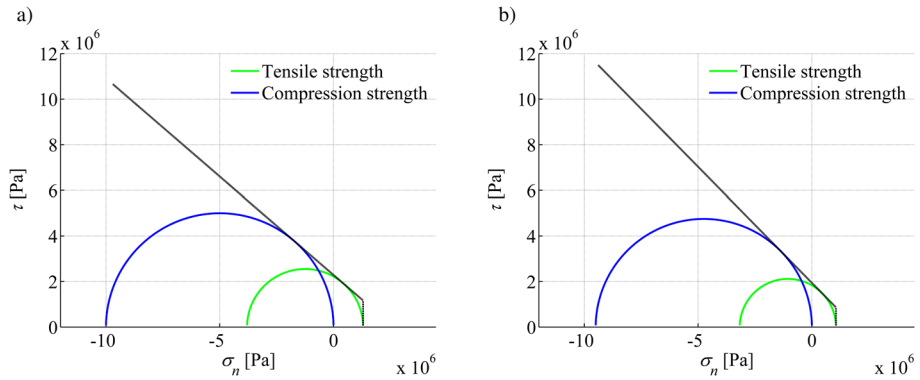

Figure 10. Uni-axial compression and tensile strengths of grouting materials: a) Silica-sand based material and b) Calcite-based material.

DOI: 10.1002/nag

which may take place in January. For the investigation, the co-axial configuration of BHE is considered because its geometry causes higher thermal resistance.

For the scenarios, two commercial product parameters of grouting materials, silica-sand-based and calcite-based, are set in calculations for the analytical model and each type of material is considered under three different geological conditions: sandstone, granite, and basalt, because of the relatively large range of selection of their parameters. The parameters of the considered rock conditions are given in Table III. The parameters of silica-sand-based and calcite-based grout materials can be found in Table I.

The calcite-based grout material has a significant difference in thermal conductivity that is considerably lower compared with the silica-sand-based grout. The differences between the rocks, which may play an important role on the development of thermal stresses, are the thermal conductivity and the stiffness of the rocks. The considered scenarios are set in an order as shown in Table IV.

7.2. *Compressive and tensile strength of grout material*

The scope of these tests is the estimation of the uni-axial compressive and tensile strengths of grouting materials with unrestricted horizontal deformation. The DIN 18–136 is followed to conduct the uni-axial compressive experiment. The associated parameters, axial strain ε and stress σ, are calculated as:

$$\varepsilon = \frac{\Delta H}{H_0} \tag{22}$$

ΔH is the vertical displacement of the piston (corresponding to the shortening of the sample) and H_0 is the initial height of the sample.

$$\sigma = \frac{F}{A_c} \quad \text{where } A_c = \frac{A_i}{1-\varepsilon} \tag{23}$$

F is the force, A_i is the initial area of the sample, while A_c is the equivalent section, different from the initial section because of the Poisson effect during compression.

In order to determine the uni-axial tensile strength of grouting materials, the Brazilian test is conducted in accordance with the standard method ASTM C 496–71. A thin circular disc is diametrically compressed until failure that occurs because of tensile stress generated along the diameter perpendicular to the compression direction. The test is valid for the materials exhibiting brittle failure.

The failure occurs where the tensile stress is the largest in the center of the specimen. At that location, tensile principal stress σ_t and compression principal stress σ_c can be expressed as a function of the applied force F, as follows [31]:

$$\sigma_t = \frac{2F}{\pi dL} \tag{24}$$

$$\sigma_c = -\frac{6F}{\pi dL} \tag{25}$$

where d is the diameter and L is the height of specimen. The obtained strength results are summarized in Table V.

Table III. Parameters of rocks used for considered scenarios.

Parameters	Sandstone	Granite	Basalt
E [Pa][a] $\times 10^9$	10	60	90
υ [−][a]	0.25	0.21	0.19
ρc [J kg^{-1} m^{-3}][b]$\times 10^6$	2.2	3	2.8
λ [W m^{-1} K^{-1}][b]	4.4	3.2	1.7

[a][27], [b][28].

DOI: 10.1002/nag

Table IV. The numbering of scenarios.

Scenarios	Sandstone	Granite	Basalt
Silica-sand based	1	2	3
Calcite based	4	5	6

Table V. The strength of grout materials.

Grout material	Silica-sand based		Calcite based	
Type of test	Brazilian tensile test	Uni-axial compression test	Brazilian tensile test	Uni-axial compression test
σ_c [MPa]	-3.8	−10	−3.17	−9.5
σ_t [MPa]	1.26	0	1.06	0

Data given in the table are provided from laboratory measurements. Each grout specimen is performed with three samples and the mean value is taken out of three samples.

7.3. *Results*

The study is carried out with the analytical solution of hollow cylinder model for a co-axial shaped pipe BHE configuration, which causes larger thermal stresses because of its geometry and thermal resistances. The calculated thermal resistances according to Eq. 21 for silica-sand-based grout is $R_{G\text{-}C1} = 0.055$ K m W^{-1}, and for calcite based grout material, $R_{G\text{-}C2} = 0.142$ K m W^{-1}. This large difference of thermal resistance accounts for the difference of the thermal conductivity of grout materials. The tangential stresses are shown in time, in accordance with the discontinuous extraction profile and plotted through 30 days at the radial distance of 0.0315 m, at the contact between the outer radius of pipe and grout, as shown in Figure 11a and b. The tangential stresses are the largest at the end of each cycle, and the value of the stress is increasing cycle after cycle. Figure 11c and d plots the radial and tangential stress components over the radial distance at the end of the 30th operation cycle. At the end of the 30th operation cycle, the tangential and the radial stresses of each scenario at the radial distance of 0.0315 m are taken into account for the strength comparison of grouting materials on failure envelope in Figure 12.

The results shown in Figure 11 demonstrate that with increasing the stiffness of rocks, the stresses on the grout materials significantly increase (i.e., from sandstone to basalt). The relationship between the thermal conductivity of the ground and of the grout causes a proportional impact on the magnitude of thermal stresses. Comparing Scenarios 1 and 4, if the thermal conductivity of ground is significantly larger than the grout, the thermal stresses that occurred on the grout increase. The results of Scenarios 3 and 6 show that the calculated stresses are nearly similar under basalt because of its lower thermal conductivity. The stresses plotted in time show that due to the higher thermal resistance of the calcite-based grout, the peak-to-peak amplitude of the stresses in time is larger than the one that occurred in the silica-sand-based grout (Figure 11a and b). This shows that a grout material that has a lower thermal conductivity causes larger differences of thermal stress between the operation and the recovery period of the ground. However, the trend of stresses in time becomes progressively stable.

Because the failure resistances are known for the two grouting materials (Figure 10), the stress state in the BHE (expressed through Mohr circles) can be compared with the failure criterion. If the stresses caused by the thermal load fall out of the failure curve, it is assumed that a failure occurs on the grouting material (Figure 12). The stress components of grout materials are taken at the end of the 30th cycle at where the maximum stress values are calculated at the radial distance of 0.0315 m for each scenario (Figure 11c and d).

The impact of the thermal stress can be seen in Figure 12, as the silica-sand based grout material is fairly close to the failure envelope under basalt (i.e., Scenario 3), as where the calcite based grout material exceeds the linear regression curve (i.e., Scenario 6).

DOI: 10.1002/nag

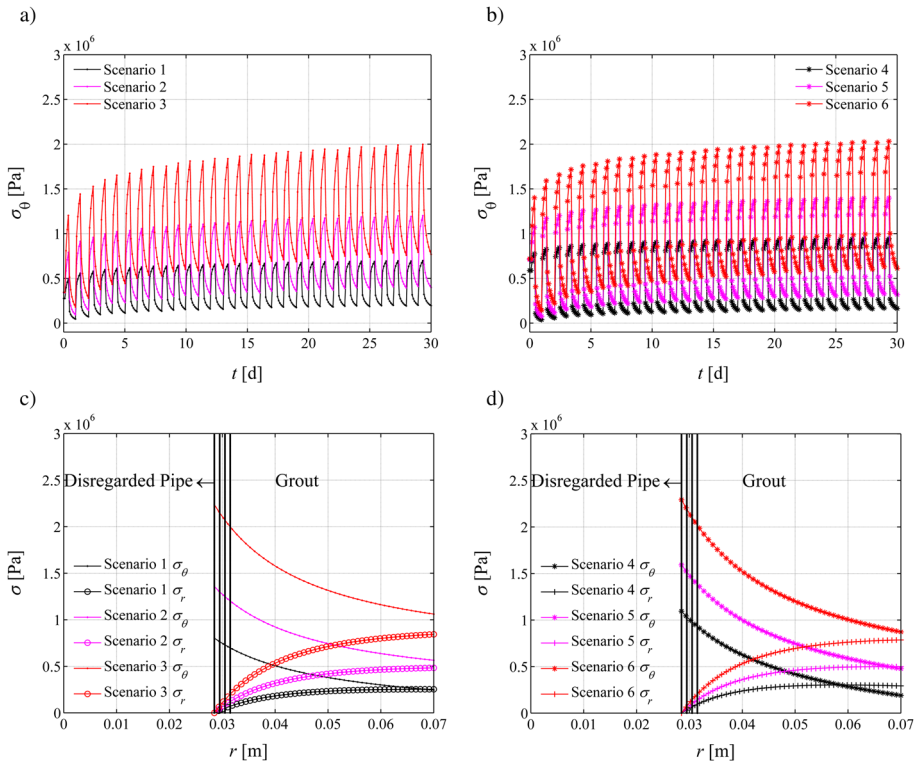

Figure 11. Stresses evolution for various scenarios for the configuration of co-axial shaped pipe borehole heat exchanger as: a) and b) tangential stresses over time at the radial distance of 0.0315 m; c) and d) stress over distance at the end of the 30th operation cycle. a) and c) denote the stresses on silica-sand based grout with the thermal resistance of 0.055 K m W^{-1}; b) and d) the stress on the calcite based grout with the thermal resistance of 0.142 K m W^{-1}.

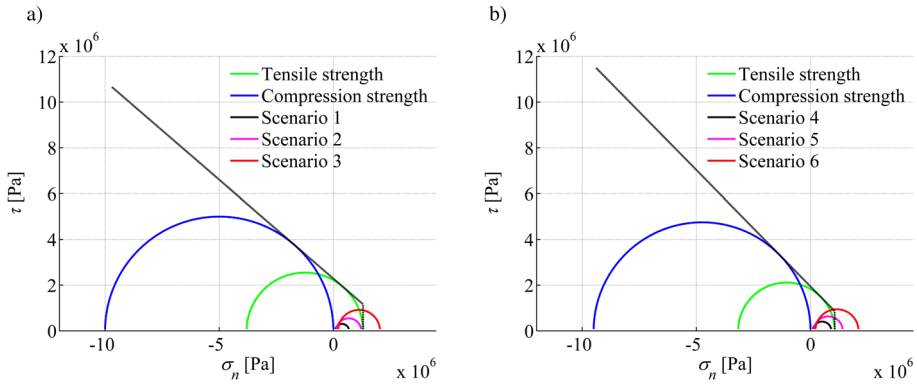

Figure 12. Comparison of failure envelope and predicted stress states under different geological conditions: a) Silica-sand based grout material. b) Calcite based grout material.

Compared with the results of the scenarios both in Figure 12a and b, the thermal stress occurred on the grout materials under sandstone (Scenarios 1 and 4) does not have a significant impact. However, under stiffer ground condition such as basalt (Scenarios 3 and 6), a failure likely occurs on the grouting material, particularly, the calcite-based grout material in basalt (Figure 12b), because of restricted contraction of BHE. Because the strength of both grout materials is nearly similar, the major reason for the possible failure of the calcite grout can be accounted to its thermal resistance, which is larger than the silica-sand grout. The impact difference between granite and basalt can be accounted, primarily, to the elastic modulus of rocks and, secondly, to the thermal conductivity of rocks. This

DOI: 10.1002/nag

thermo-mechanical behavior can be explained, as the lower thermal conductivity of basalt increases the thermal gradient and causes a larger contraction of the grout material. However, due to the stiffness of basalt, this contraction is limited and, therefore, the tensile forces raise the stresses on the grout. Finally, it is also worth to mention that upon heating scenarios, the situation would be much less critical because the constrained thermal expansion generates compressive stresses in the BHE. The grout strength being much higher in compression than in tension, it would not lead to BHE failure.

8. CONCLUSION

The grouting material used for the installation of a BHE must ensure durability against dilatation or contraction because the mechanical interaction between the grouting material and the surrounding ground becomes important because of heating and cooling operations of a building. Numerical and analytical studies are carried out for predicting the thermo-mechanical behavior of a BHE. The combination of miscellaneous analytical models provides a comprehensive solution to evaluate such a complex thermo-mechanical problem due to both the model configurations and the heat loading profile.

According to the results, the impact of thermal stress is attributed to the magnitude of thermal loading (i.e., temperature gradient between the BHE and the subsurface), the ground conditions, and the thermo-physical characteristics of grout material. As the most sensitive parameter to the thermo-mechanical behavior of subsurface, the stiffness of the ground plays a major role to increase the thermal stresses in a BHE because of restricted deformation. We observe also that the lower thermal conductivity of the grout material slightly increases the stresses because of its higher thermal resistance that induces a thermal gradient in the BHE. On the other hand, the stiffness of the grout may induce stresses, but its larger stiffness conversely increases the strength of the material resisting to a possible failure.

This study reveals that the thermal demand from the ground must be scheduled in such a way that it fulfills the requirement for the mechanical resistance of the BHE. Even if BHE has, a priori, no structural role (by opposition to heat exchanger piles), internal stresses induced by the thermal loading may generate failure of the BHE, leading to a loss of integrity of the system and an undesired increase of permeability. In particular, in case of under stiff rock formations, if the ground also has a lower thermal conductivity such as basalt, it is appropriate for heating and cooling purposes to operate BHEs with an optimum heat extraction rate of not more than $50\,\mathrm{W\,m^{-1}}$. A grout material which has an equivalent thermal conductivity to the rock formation can be preferable for a possible installation in order to minimize thermal gradient inside BHE.

9. NOMENCLATURE

E	Young's modulus (Pa)
c	specific heat capacity ($\mathrm{J\,kg^{-1}\,K^{-1}}$)
H	borehole length (m)
Rc	unit length borehole resistance ($\mathrm{K\,m\,W^{-1}}$)
r_a	inner radius of cylinder (m)
r_b	outer radius of cylinder (m)/radius of the borehole (m)
r_p	outer radius of pipe (m)
q_L	specific heat exchange rate per unit length of borehole ($\mathrm{W\,m^{-1}}$)
t	time (s)
T	temperature (°C)
ΔT	temperature difference (°C)
x, y, z	space coordinates (m)
x_c	half-shank distance of U-shaped pipe borehole heat exchanger (m)

9.1. Greek symbols

α	linear thermal expansion coefficient ($\mathrm{K^{-1}}$)

DOI: 10.1002/nag

ε_θ	tangential strain (−)
ε_r	radial strain (−)
λ	thermal conductivity ($\mathrm{W\,m^{-1}\,K^{-1}}$)
ρ	mass density ($\mathrm{kg\,m^{-3}}$)
σ_θ	tangential stress (Pa)
σ_r	radial stress (Pa)
σ_c	compression strength (Pa)
σ_t	tensile strength (Pa)
τ	shear strength (Pa)
υ	Poisson's ratio (−)

9.2. *Subscripts*

C	co-axial pipe borehole heat exchangers
G	grout
R	rock
U	single U-shaped pipe borehole heat exchanger

Appendix: A

In this section, the derivation of the displacement is demonstrated. The strain particular solutions given in Eq. 2 are replaced into the stress components (Eqs. 3 and 4) afterwards setting the stress equations into the momentum equilibrium equation (Eq. 1):

$$\frac{\partial^2 u_r}{\partial r^2}+\frac{1}{r}\frac{\partial u_r}{\partial r}-\frac{1}{r^2}u_r=\alpha\frac{\partial \Delta \mathrm{T}}{\partial r}(1+v) \tag{A1}$$

This equilibrium equation reduces to:

$$\frac{\partial}{\partial r}\left(\frac{1}{r}\frac{\partial}{\partial r}(ru_r)\right)=\alpha\frac{\partial \Delta \mathrm{T}}{\partial r}(1+v) \tag{A2}$$

After two integrations with respect to r, and by changing the indefinite integral into definite with the boundaries of a circular ring with inner radius r_0 and outer radius r, subjected to axisymmetric temperature change $\Delta \mathrm{T} = \Delta \mathrm{T}(r)$, the total displacement can be obtained as:

$$u_r(r)=\frac{(1+v)\alpha}{r}\overbrace{\int_{r_0}^{r}\Delta \mathrm{T}\tau d\tau}^{\mathrm{S}}+Ar+\frac{B}{r} \tag{A3}$$

where A and B are the integral constants. At this point, the particular solutions of strain components can be solved as:

$$\varepsilon_r=\frac{\partial u_r}{\partial r}=(1+v)\alpha\Delta \mathrm{T}-\frac{(1+v)\alpha S}{r^2}+A-\frac{B}{r^2} \tag{A4}$$

$$\varepsilon_\theta=\frac{1}{r}\left(\frac{\partial u_\theta}{\partial \theta}+u_r\right)=\frac{u_r}{r}=\frac{(1+v)\alpha S}{r^2}+A+\frac{B}{r^2} \tag{A5}$$

Appendix: B

The integral constants are obtained, depending on the boundary conditions defined in Section 2, to calculate the stresses that occurred in the grout. The unknown constants will be determined in two regions, in the grout and in the rock, and the constants and parameters are subscripted as G, denoting the grout and R in the rock.

DOI: 10.1002/nag

(i) Assuming the boundary condition as the stress at the inner radius r_a is zero, the constant B_G can be related to A_G as:

$$\sigma_r(r_a) = 0 \Rightarrow B_G = A_G r_a^2 \frac{1+\nu_G}{1-\nu_G} \tag{B1}$$

(ii) In the far field, in the rock, when r tends to infinity, the displacement is assumed to vanish. Consequently, from Eq. A3, we can deduce that $A_R = 0$.

(iii) The grout hollow cylinder is surrounded by an infinite ground. By assuming equality of displacement at the interface between the two materials, $u_{r,G}(r_b) = u_{r,R}(r_b)$, the stress components in the grout can be evaluated, depending on the mechanical properties of the surrounding rock. In the grout, when B_G is expressed as a function of A_G (Eq. B1), Eq. A3 gives:

$$u_{r,G}(r_b) = \frac{(1+\nu_G)\alpha_G S_G(r_b)}{r_b} + A_G\left(r_b + \frac{r_a^2}{r_b}\frac{1+\nu_G}{1-\nu_G}\right) \tag{B2}$$

and in the rock:

$$u_{r,R}(r_b) = \frac{(1+\nu_R)\alpha_R \overbrace{S_R(r_b)}^{=0}}{r_b} + \frac{B_R}{r_b} \tag{B3}$$

The equality of displacements at the interface leads to:

$$u_{r,G}(r_b) = u_{r,R}(r_b) \Rightarrow B_R = A_G\left(r_b^2 + \frac{r_a^2(1+\nu_G)}{1-\nu_G}\right) + (1+\nu_G)\alpha_G S_G(r_b) \tag{B4}$$

(iv) Similarly, to determine the stress equilibrium at the interface $\sigma_{r,R}(r_b) = \sigma_{r,G}(r_b)$ by using Eq. 5, when B_G is expressed as a function of A_G (Eq. B1), the stress occurred in the grout is:

$$\sigma_{r,G}(r_b) = \frac{E_G}{r_b^2}\left[\frac{A_G\left(r_b^2 - r_a^2\right)}{(1-\nu_G)} - \alpha_G S_G(r_b)\right] \tag{B5}$$

The stress occurred in the rock can be also obtained in Eq. 5, replacing B_R as a function of A_G (Eq. B4):

$$\sigma_{r,R}(r_b) = -\frac{E_R}{r_b^2}\left[\alpha_R S_R(r_b) + \frac{A_G}{(1+\nu_R)}\left(r_b^2 + \frac{r_a^2(1+\nu_G)}{1-\nu_G}\right) + \frac{(1+\nu_G)}{(1+\nu_R)}\alpha_G S_G(r_b)\right] \tag{B6}$$

Afterwards, by using the equilibrium $\sigma_{r,G}(b) = \sigma_{r,R}(b)$, the constant A_G is determined as:

$$\sigma_{r,G}(r_b) = \sigma_{r,R}(r_b) \Rightarrow A_G = \frac{\alpha_G S_G(r_b)[E_G - E_R(1+\nu_G)]}{\left[\frac{E_G\left(r_b^2 - r_a^2\right)}{(1-\nu_G)} + \frac{E_R\left(r_b^2 + \frac{r_a^2(1+\nu_G)}{(1-\nu_G)}\right)}{(1+\nu_R)}\right]} \tag{B7}$$

Thus, by setting the constants in the considered equations, Eqs. 5 and 6, the radial and tangential stress components in the grout can be evaluated, depending on the mechanical properties of the surrounding rock.

DOI: 10.1002/nag

REFERENCES

1. Laloui L, Nuth M, Vulliet L. Experimental and numerical investigations of the behaviour of a heat exchanger pile. *International Journal for Numerical and Analytical Methods in Geomechanics* 2006; **30**(8):763–781.
2. Bourne-Webb PJ, Soga K, Amis T, Davidson C, Payne P, Amatya B. Energy pile test at Lambeth College, London: geotechnical and thermodynamic aspects of pile response to heat cycles. *Geotechnique* 2009; **59**(3):237–248.
3. Amatya BL, Soga K, Bourne-Webb PJ, Amis T, Laloui L. Thermo-mechanical behaviour of energy piles. *Geotecnique* 2012; **62**(6):503–519.
4. Di Donna A, Dupray F, Laloui L. Numerical study of the heating-cooling effects on the geotechnical behaviour of energy piles. In Coupled Phenomena in Environmental Geotechnics, Musso G, (ed.). CRC Press: London, 2013; 475–482.
5. Laloui L, Mimouni T, Dupray F. Advances in the analysis of thermo-active foundations. In Coupled Phenomena in Environmental Geotechnics, Musso G, (ed.). CRC Press: London, 2013; 85–102.
6. Allan M, Philippacopoulos A. Performance characteristics and modelling of cementitious grouts for geothermal heat pumps, 2000; pp. 3355–3360.
7. Philippacopoulos AJ, Berndt ML. Structural analysis of geothermal well cements. *Geothermics* 2002; **31**(6): 657–676.
8. Kanj M, Abousleiman Y. Porothermoelastic analyses of anisotropic hollow cylinders with applications. *International Journal for Numerical and Analytical Methods in Geomechanics* 2005; **29**(2):103–126.
9. Shao ZS. Mechanical and thermal stresses of a functionally graded circular hollow cylinder with finite length. *International Journal of Pressure Vessels and Piping* 2005; **82**(3):155–163.
10. Shao ZS, Ma GW. Thermo-mechanical stresses in functionally graded circular hollow cylinder with linearly increasing boundary temperature. *Composite Structures* 2008; **83**(3):259–265.
11. Radu V, Taylor N, Paffumi E. Development of new analytical solutions for elastic thermal stress components in a hollow cylinder under sinusoidal transient thermal loading. *International Journal of Pressure Vessels and Piping* 2008; **85**(12):885–893.
12. Shonder JA, Beck JV. Determining effective soil formation thermal properties from field data using a parameter estimation technique. *ASHRAE Transactions* 1999; **105**:458.
13. Beier RA, Smith MD. Analyzing interrupted in-situ tests on vertical boreholes. *ASHRAE Transactions* 2005; **111**(1):702–713.
14. Slaughter WS. The Linearized Theory of Elasticity. Birkhaeuser: Boston, 2002.
15. Boley BA, Weiner JH. Theory of Thermal Stresses, vol. **270**(4). John Wiley & Sons: New York, 1960; p. 586.
16. Faupel JH, Fisher FE. Engineering Design : A Synthesis of Stress Analysis and Materials Engineering. J. Wiley and Sons: New York, N.Y., 1981.
17. Gehlin S. PhD. Thesis thermal response test, Luleå University of Technology, Luleå: Sweden, 2002.
18. Bejan A, Kraus AD. Heat Transfer Handbook. John Wiley & Sons Inc.: Hoboken, New Jersey, 2003; 1480.
19. Hellström G. Thermal performance of borehole heat exchangers, 1998, The Second Stockholm International Geothermal Conference.
20. VDI-Richtlinie. Thermal use of the undergorund - GSHP systems, VDI 4640 Blatt 2. Verain Deutscher Ingenieure, VDI-Verlag, Düsseldorf, 2001.
21. Erol S, Hashemi MA, François B. Analytical solution of discontinuous heat extraction for sustainability and recovery aspects of borehole heat exchangers. *International Journal of Thermal Sciences* 2015; **88**:47–58.
22. Fei Y. Thermal expansion. In Mineral Physics and Crystallography - A Handbook of Physical Constants, AGU Reference Shelf 2, Ahrens TJ (ed.). American Geophysical Union: Washington, USA, 1995; 29–44.
23. Ineos. Handling book for technical properties of high density polyethylene. INEOS Olefins & Polymers USA, 2009. [Online]. Available: www.ineos-op.com. [Accessed: 08-Oct-2013].
24. Erol S, François B. Efficiency of various grouting materials for borehole heat exchangers. *Applied Thermal Engineering* 2014; **70**(1):788–799.
25. Hakagerodur. Hakagerodour-geothermal: handling book for borehole heat exchangers technical details of geothermal pipes; model: geotherm PE-100, *HakaGerodur AG, Benken, CH All*, 2010.
26. Skinner BJ. Thermal expansion. In Handbook of Physical Constants, Clark SP Jr. (ed.). Revised Ed. The Geological Society of America, Inc.: New York, Memoir 97, 1966; pp. 75–96.
27. De Vallejo LIG, Ferrer M. Geological Engineering. CRC Press / Balkema: AK Leiden, Netherlands, 2011; 153.
28. VDI-Richtlinie. Thermal use of the undergorund - fundamentals, aprovals and environmental aspects, VDI 4640 Blatt 1. Verain Deutscher Ingenieure, VDI-Verlag, Düsseldorf, 2000; pp. 9–10.
29. Bennet J, Claesson J, Hellström G. Multipole method to compute the conductive heat flows to and between pipes in a composite cylinder. *Notes Heat Transf.*, 1987.
30. Collin F, Cui YJ, Schroeder C, Charlier R. Mechanical behaviour of Lixhe chalk partly saturated by oil and water: experiment and modelling. *International Journal for Numerical and Analytical Methods in Geomechanics* 2002; **26**(9):897–924.
31. Li D, Wong LNY. The Brazilian disc test for rock mechanics applications: review and new insights. *Rock Mechanics and Rock Engineering* 2013; **46**(2):269–287.

DOI: 10.1002/nag